

# Cooperative caging and transport using autonomous aquatic surface vehicles

Filippo Arrichiello · Hordur K. Heidarsson ·  
Stefano Chiaverini · Gaurav S. Sukhatme

Received: 15 March 2011 / Accepted: 19 November 2011 / Published online: 17 December 2011  
© Springer-Verlag 2011

**Abstract** We present a study on the cooperative control of two autonomous surface vehicles performing a caging and transport mission on the water surface. The two vehicles, connected to each other by means of a floating flexible rope, are required to capture a floating target from a given location, and transport it to a designated position. We focus on the coordination and control strategy to meet these requirements, and on its implementation on two under-actuated vehicles. We describe a multi-layered control architecture which achieves the goal, followed by simulation studies and field experiments with the two vehicles caging and transporting a floating target on the surface of a lake.

**Keywords** Marine robotics · Cooperative control · Cooperative caging · Field robotics

**Electronic supplementary material** The online version of this article (doi:10.1007/s11370-011-0104-9) contains supplementary material, which is available to authorized users.

A preliminary version of this paper was published in the proceedings of the 2010 IEEE International Conference on Robotics and Automation [13].

F. Arrichiello (✉) · S. Chiaverini  
Dipartimento di Automazione, Elettromagnetismo, Ingegneria dell'Informazione e Matematica Industriale, Università degli Studi di Cassino, Via G. Di Biasio 43, 03043 Cassino (FR), Italy  
e-mail: f.arrichiello@unicas.it

S. Chiaverini  
e-mail: chiaverini@unicas.it

H. K. Heidarsson · G. S. Sukhatme  
The Robotic Embedded Systems Laboratory, University of Southern California, Los Angeles, CA, 90089, USA  
e-mail: heidars@usc.edu

G. S. Sukhatme  
e-mail: gaurav@usc.edu

## 1 Introduction

Aquatic robots hold the promise of a wide range of applications ranging from harbor security to remote ocean science. Here, we focus on a particular mission—target capture and transport—to be carried out by autonomous surface vehicles (ASVs)—small ( $\sim 2\text{ m}$ ) autonomous robotic boats that move on the water's surface.

Automatic motion control problems for individual ASVs have been widely investigated in the literature. A comprehensive treatment of the main issues in guidance, navigation and control of ASVs is available in [25]. Motion control problems e.g., tracking control and dynamic positioning for fully actuated vehicles are well-understood. For under-actuated vehicles, i.e., those unable to apply forces in all directions, tracking control approaches have been investigated in [2, 14, 30], as have dynamic positioning techniques in [3, 34, 35].

Several studies have dealt with ASV fleets; most focusing on the formation control problem. The work in [16] deals with the formation control problem for under-actuated ASVs with communication constraints and solves this via non-linear techniques. In [28], a technique that uses Lagrange multipliers to solve the formation control problem in the presence of slowly varying environmental disturbances and measurement noise is presented. The work in [23] employs a sliding mode technique for the formation control of a team of under-actuated ASVs, while the work in [20] uses an approach based on graph theory to control a formation of under-actuated ASVs considering information exchange. Recent work in [27] deals with the coordinated control of a fleet of under-actuated ASVs, subject to constant disturbances, executing cooperative path following.

Despite the recent activity in ASV-related research, experiments with real vehicles in the field are limited. Notable exceptions include [1, 12, 15, 19, 37]. In particular, in [19], a

fleet of ASVs developed at the MIT Department of Ocean Engineering, and its usage for experiments on collision avoidance and coordinated navigation are presented; in [37], the same fleet of ASVs is used to perform searching missions in a given area. In [1], simulations and experiments in open sea of joint motion with two surface vehicles are presented. In [15], experiments of reactive obstacle avoidance algorithms in Singapore harbor are presented. In [12], we presented experiments of cooperative navigation with two ASVs while satisfying a communication constraint.

Here we present a study on the use of a cooperating duo of ASVs, connected by a floating rope, to execute a capture and transport mission on the water's surface. This problem is motivated by applications in payload deployment (e.g., deployment of buoys or marine sensor network nodes), automatic rescue (e.g., transporting a human or failed ASV to safety) and construction (e.g., building floating docks in a harbor). Moreover, similar missions can be performed to clean the water's surface (e.g., notably in the case of oil skimming where the objective is to corral and transport a deformable oil slick instead of a rigid object) or collect material for biological investigation. Since we use a rope to capture the target, we will refer to the process of capture as caging. In particular, we consider the problem of requiring two under-actuated ASVs to capture a floating object (henceforth, the target) from a known initial location and transport it to a designated destination (henceforth, the goal) as shown in Fig. 1.

In the literature, the problem of caging and transport by multiple robots has been solved using multiple vehicles pushing/pulling the object from different contact points, and a significant amount of literature covers most of the main aspects of the problem for wheeled multi-robot systems [18,24,26,29,38]. An approach for a swarm of autonomous tugboats to cooperatively move a large object on the water has been recently presented in [21,22]; the proposed approach is tested in simulation and with preliminary experiments where bi-

directional thruster rigidly attached to the hull to simulate push/pull effects of the tugboats. To the best of our knowledge, our paper is one of the first papers focusing on caging in an active medium, such as the water surface, where the vehicles do not refer on push/pull strategies but use a flexible rope to tow an object. Moreover, it is also one of the few applications of cooperating ASVs in the field and the first instance of target capture and transport by two ASVs operating in tandem.

Our technical focus is on the coordination control strategy for the under-actuated ASVs. The control architecture onboard each vehicle is organized into layers operating at different frequencies. At the highest level, a supervisor, using both sensor data local to the vehicle and receiving information from the other vehicle, dynamically defines the active behaviors and their priority order. At an intermediate level, the Null-Space-based Behavioral (NSB) control method [5,8] is used to merge the multiple behaviors organized by priority and to define the motion directives. Finally, a low-level control (LLC), specific to the ASVs used in the experiments described here, generates the thruster and rudder commands to realize the motion directives received from the NSB. The LLC also compensates for the hydrodynamic effects of the floating rope as it is dragged across the water surface.

The control approach has been tested through numerical simulations and experiments in the field. For the experiments, two ASVs were attached to each other with a floating rope to capture the target from a known position and relocate it to the goal. The numerical simulations and the experimental results validate the proposed strategy and represent the first realization of a capture and transport mission via caging in an aquatic setting.

This paper extends the results reported in [13] that summarized preliminary work on the coordination control strategy for ASVs performing the caging mission. In this paper,



**Fig. 1** Two autonomous surface vehicles cooperatively caging an object floating on a lake surface

we present for the first time a complete caging experiment using a real floating rope; we also give a hydrodynamic analysis to estimate the forces applied by the floating rope to the ASV hull, and the consequent modifications made to the low-level control. In fact, in [13] the only coordination strategy was tested, the target was not really caged since we did not effectively use the floating rope in experiments and the hydrodynamic effects of the rope were neglected in the control. Moreover, as a matter of practicality, the experiments reported here employ a fault management strategy for the supervisor to manage the ‘target missing’ case. The experiments were performed with a target equipped with GPS. These features were absent in [13].

It may be noted that the two ASV experimental testbed used here is the same as the one used for the cooperative mission described in [12], wherein two ASVs were required to cooperatively visit several locations distributed in the environment while subject to a communication constraint. For the mission considered here, new behavior functions were built to solve the specific problem of the caging mission with under-actuated vehicles and a new coordination control strategy is proposed (relative to what was used in [12]). Moreover, since the experiments reported in [12], the internal software architecture of the ASVs has been completely revised and now uses the Robot Operating System (ROS) framework [36].

The rest of the paper is organized as follows. Section 2 describes the mission to be performed and the multi-layered control architecture to accomplish it. Sections 3, 4 and 5 respectively describe each of the control layers: the Supervisor, the NSB control and the Low-Level Control. Section 6 describes the results from the simulation of the mission. Section 7 presents the experimental results from an execution of the caging mission in the field with two ASVs connected with a floating rope caging an object on a lake surface. Finally, Sect. 8 summarizes the conclusions and sketches directions for future work.

## 2 Mission and control architecture

In the proposed mission, we require two under-actuated ASVs to capture a target and transport it to a goal. The vehicles are attached to each other with a floating flexible rope (see the sketch in Fig. 2), thus their motions have to be coordinated in such a way that the target is captured and retained during the transport. To complete the mission, the following assumptions are made:

- The rope, though flexible, is of constant length; it does not elongate nor is it payed out.
- The environment is free of external obstacles. Avoidance of external obstacles will be added in future research, it is not within the scope of this paper.

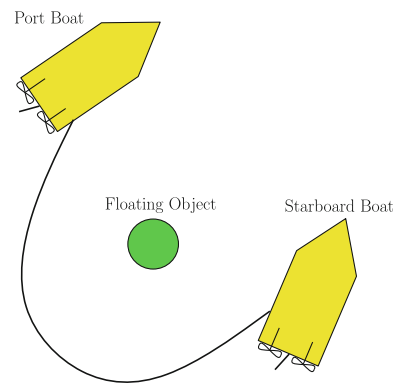


**Fig. 2** Sketch of cooperative caging with two surface vehicles connected with a floating rope

Under these assumptions, the following constraints need to be satisfied:

- To avoid losing the target during transport, backward motion of the formation is prohibited.
- At all times, the distance between the vehicles must be less than the (constant) rope length.
- The vehicles must not cross each other (to avoid twisting the rope and preventing it from getting tangled in the propellers).

While satisfying these constraints, the ASVs achieve their primary objective to cage and transport the target controlling the following variables of interest:

- The relative positions of the vehicles, as a formation, have to be controlled. We control the geometric center of the two vehicles (since the vehicles are identical this amounts to controlling their centroid) causing it move toward either the target or the goal as appropriate.
- Designating one vehicle as the port vehicle and the other as the starboard vehicle, we define the angle and the advancing direction of the formation. We control this angle to ensure that the vehicles approach the target with the correct orientation. Moreover, to avoid losing the target during transport, backward motion of the formation is prohibited.
- Since the vehicles must avoid collisions among themselves, we control their relative distance.

We decompose the overall mission is in a logic sequence of stages, and organize the control architecture into a layered structure, sketched in Fig. 3, where each of the three layers focuses on a different aspect of the overall control problem.

At the highest level, a supervisor on board each vehicle defines, for each stage of the mission, the task of the system and, using both sensor data and the information received from

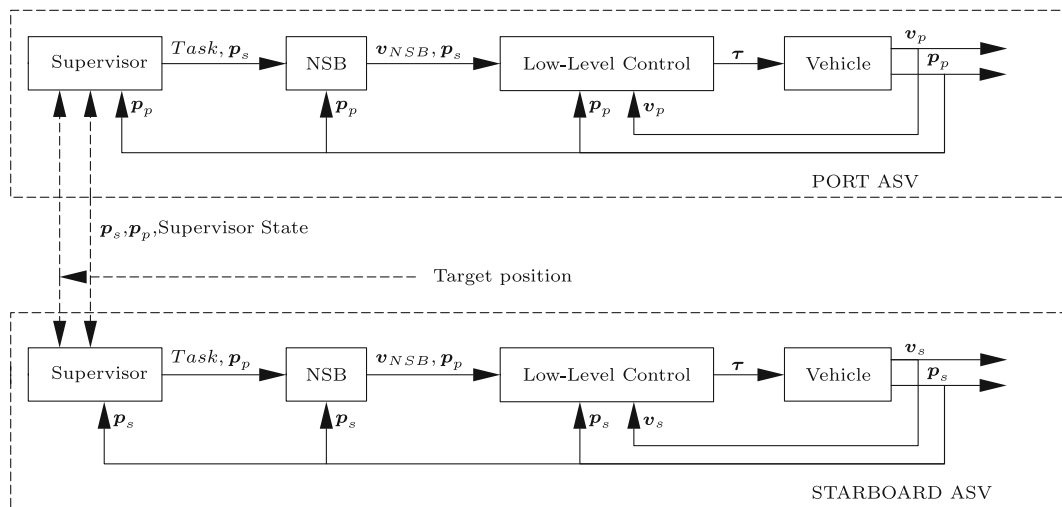


**Fig. 3** Control architecture for a team of two under-actuated vehicles

the other vehicle, manages the transitions from one stage to the following. The task is defined by assigning a set of active elementary behaviors (whose concept will be clarified in the following) and their reference values.

The task is managed by the intermediate control level and it is achieved by controlling a set of variables of interest to assume proper values. Referring to behavior-based robotic approaches (e.g., see [10]), each of the controlled variables generates an elementary behavior (or, simply, behavior), i.e. a motion command to the robot with the aim of achieving a specific goal. However, since generally a unique motion command to the robot that simultaneously generates all the behaviors does not exist, the behaviors are combined with a proper coordination strategy. In this paper, we use the NSB control described in Sect. 4 to appropriately combine the behaviors in order of priority. Operationally, each of the previous variables of interest and constraints are encoded into a proper set of behaviors:

- (a) centroid position,
- (b) orientation of the formation,
- (c) distance between the vehicles,
- (d) cross avoidance,
- (e) collision avoidance.

The NSB combines the functions associated with the active behaviors in order to define the motion directives to the ASV, e.g., the desired velocity and heading angle.

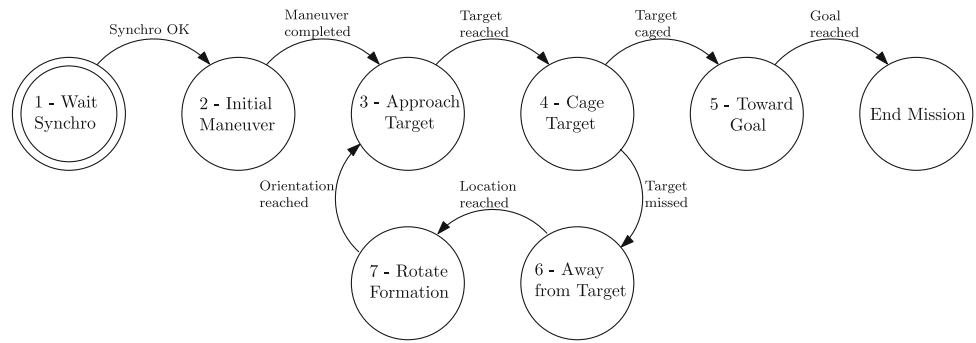
At the last layer of the control architecture, a Low-Level Controller, specifically designed for the testbed vehicles and adjusted for the specific caging and transport tasks, generates the thruster and rudder commands from the motion directives received from the NSB.

### 3 Supervisor

The supervisors of the two ASVs manage the overall mission execution by defining, for each stage of the mission, the behaviors that have to be activated in order to achieve the associated task. In particular, the supervisors manage the communication between the ASVs and select the active behaviors and their desired values based on both vehicles' sensor data and the target position (in this paper we suppose that the target directly communicates its position to the ASVs). The supervisor also defines if and when a behavior of the associated task has to subsume a lower priority one, and it is in charge of managing the transitions from one stage to following. With this in mind, the supervisor is organized as a Finite State Machine that, for the mission considered here, is composed as shown in Fig. 4. Referring to this Figure, the states can be described as:

1. *Wait synchro*: initialize the system and wait until the other vehicle has been initialized,
2. *Initial maneuver*: perform an initialization maneuver to make the floating rope assume an appropriate configuration that keeps it in tension,
3. *Approach target*: approach the target with an appropriate formation angle,
4. *Cage target*: cage the target by overtaking it and causing the formation to keep its orientation constant,
5. *Toward goal*: move the formation toward the goal, avoiding maneuvers that may cause the target to be lost,
6. *Away from target*: if the target has not been captured move away from it before trying to cage it again,
7. *Rotate formation*: rotate the formation to approach the target from an angle better suited for capture.

**Fig. 4** Supervisor states for the caging-based capture and transport mission



In a general case, the supervisor may dynamically define the priority order of the behaviors for a specific task, however, in this specific case the behaviors are organized respecting the fixed, following priority order:

1. Collision avoidance,
2. Distance between the vehicles,
3. Cross avoidance,
4. Orientation of the formation,
5. Centroid position.

This order arises from the following safety and practical considerations. Collision avoidance is of primary importance to preserve the vehicles’ integrity; the control of the inter-vehicle distance preserves the integrity of the floating rope. The cross avoidance is then chosen as the next most important behavior since it is necessary to ensure the proper mission execution and to avoid the rope getting stuck in the vehicles’ thrusters. The formation orientation angle control is needed to ensure that the target is approached from a direction appropriate for capture and transport, and finally the centroid is controlled to move the formation toward the goal—thereby achieving transport. When a behavior is deactivated, it is deleted from the previous priority list while the lower-priority behaviors shift one step up. For each task, the active behaviors are listed in Table 1, while their desired reference values are explained in the simulation and experimental results sections. It is worth noting that behaviors as collision avoidance,

distance between the vehicles and cross avoidance are considered active but they take effect only in specific conditions (e.g., when the distance between the ASVs is lower than a given threshold).

On board each vehicle, the transition from one state to another depends either on threshold values associated with behavior function errors or on the supervisor state of the other vehicle. This latter dependence has been added because the vehicles communicate asynchronously, and the measured function behavior errors can differ slightly between the two vehicles due to sensor noise. Thus, as soon as one of the supervisors reads that the desired threshold value used to switch to the following state has been reached, both the supervisors have to switch to the respective next states. This is achieved by communication instead of local sensing.

The description of the supervisors’ state transition will be clarified in the simulation results section, where each state behavior is discussed in detail.

#### 4 NSB and behaviors for the caging mission

The Supervisor dynamically sends the list of active behaviors and their priority order to the NSB control, which is a particular behavior-based approach developed by some of the authors of this paper. The main idea of the approach is to define a function for each behavior and to use a projection mechanism (based on the Null-Space projection matrix) to compose these behaviors following their priority order. The behaviors are combined so that the lower priority behaviors do not affect the higher priority ones. The Null-Space projection matrix of a behavior filters out the velocity component of the lower priority ones that would affect its functionality. A detailed description of this approach extends beyond the scope of this paper, but can be found in [4–6, 8]. In particular, the basic concepts of the NSB technique and a comparison with the main behavior based approaches (such as [9, 17]) can be found in [6]; referring to [10], in fact, the NSB technique differs from the other existing methods in the behavioral coordination, i.e., in the way the outputs of the single behaviors are combined to achieve the task. Experimental

**Table 1** Active behaviors for each task

	Coll.	Dist.	Cross	Orient.	Cent.
1-Wait synch.	No	No	No	No	No
2-Init. man.	Yes	Yes	Yes	No	Yes
3-Appr. target	Yes	Yes	Yes	Yes	Yes
4-Cage target	Yes	Yes	Yes	Yes	Yes
5-Toward goal	Yes	Yes	Yes	Yes	Yes
6-Away target	Yes	Yes	Yes	No	Yes
7-Rot. form.	Yes	Yes	Yes	Yes	No
End mission	No	No	No	No	No



where  $J_b \in \mathbb{R}^{2 \times 4}$  is the Jacobian matrix defined as

$$J_b = \frac{1}{2} \begin{bmatrix} 1 & 0 & 1 & 0 \\ 0 & 1 & 0 & 1 \end{bmatrix},$$

where  $\tilde{\sigma}_b = \sigma_{b,des} - \sigma_b$  is the error behavior function, and  $J_b^\dagger = J_b^T (J_b J_b^T)^{-1}$  is the pseudo-inverse of the Jacobian matrix. The desired value of the behavior function ( $\sigma_{b,des}$  and  $\dot{\sigma}_{b,des}$ ) expresses the desired trajectory of the centroid.

### 4.2 Orientation

The orientation behavior function controls the angle of the formation. Referring to Fig. 5, it controls the angle  $\phi$  that represents the advancing direction of the formation. Thus, the behavior function is defined as:

$$\sigma_o = \text{atan2}(\Delta Y, \Delta X) + \frac{\pi}{2},$$

where  $\Delta Y, \Delta X$  are the projections along Y and X of the vector  $p_s - p_p$ .

The Jacobian matrix is calculated as

$$J_o = \frac{1}{\|p_s - p_p\|^2} \begin{bmatrix} p_s[1] - p_p[1] \\ -(p_s[0] - p_p[0]) \\ -(p_s[1] - p_p[1]) \\ p_s[0] - p_p[0] \end{bmatrix}^T,$$

and the output is elaborated as:

$$v_o = J_o^\dagger (\dot{\sigma}_{o,d} + \lambda_o \tilde{\sigma}_o). \tag{7}$$

### 4.3 Collision-avoidance

The collision-avoidance behavior is implemented individually on the two vehicles. In the following, we describe the behavior function for the starboard vehicle (the description for the other vehicle is straightforward). In the presence of the port vehicle (considered as a static obstacle) in the advancing direction, the goal of the behavior is to keep the starboard

vehicle at a safe distance from the port vehicle. Thus, its implementation produces a velocity in the  $p_s - p_p$  direction to control the inter-vehicle distance (in a radial direction if considering a circle centered in  $p_p$ ). Formally, the behavior function is

$$\sigma_c = \|p_s - p_p\| \in \mathbb{R},$$

where  $J_c = \hat{r}^T \in \mathbb{R}^{1 \times 2}$  is the behavior Jacobian where  $\hat{r} = \frac{p_s - p_p}{\|p_s - p_p\|}$  is the unit vector aligned with the  $p_s - p_p$  direction. Defining  $\sigma_{c,d} = d$  as the desired distance, the behavior output is

$$v_c = J_c^\dagger \lambda_c (d - \|p_s - p_p\|). \tag{8}$$

Possible motions in this behavior null-space are all the motions that do not change the distance between the vehicles. Thus, considering a circle centered in  $p_p$  and passing through  $p_s$ , the null-space projector matrix filters out the velocity components of the lower-priority behaviors in the radial direction, while allowing the components in the tangential direction (see [6]).

### 4.4 Distance

This distance behavior function controls the distance between the vehicles to ensure that the rope does not break. The behavior function is formally equivalent to collision-avoidance, however it is activated under different conditions (i.e., when the inter-vehicle distance is greater than a given threshold). It also has different desired values and behavior function gains.

### 4.5 Cross avoidance

This behavior is designed to prevent the vehicles from crossing each other to avoid twisting the rope (see Fig. 6). Accordingly, referring to Fig. 5b, the behavior output velocity vector for the starboard vehicle is computed as a function of the



**Fig. 6** a Sketch of the twisted rope situation. b Twisted condition with the real vehicles. The rope in the picture is highlighted to easily recognize its shape

angle  $\theta$  (computed positive in the clockwise direction looking down on the water surface from above). The behavior function and null-space projection matrix are built geometrically. For example, considering the position, in polar coordinates, of the starboard vehicle in the reference frame of the port vehicle, the behavior function outputs a velocity in the opposite direction to the  $Y_p$  axis when  $0 < \theta < \pi/2$  and when  $\pi/2 < \theta < \pi$  (i.e., when the  $Y$  component of  $\mathbf{p}_s$  in port vehicle reference system is positive). The velocity in the  $X_p$  direction is generally not controlled and this degree of freedom is used to build the null-space projection matrix. However, when the starboard vehicle is close to the positive  $Y_p$  semi-axis ( $\theta \sim \pi/2$ ), the  $X_p$  direction is controlled in order to avoid crossing of the vehicles. For the port vehicle an analogous procedure is used. If the rope becomes twisted, an emergency procedure is activated.

## 5 Low-level control

The low-level control (LLC) steers the vehicle in a desired direction and moves it with a desired velocity [25]. When a motion reference command is received from the NSB, the LLC generates actuator commands. The ASVs used for our experiments have two independent thrusters (see Fig. 5a) that can be used to apply a force in the surge direction and a torque to change the vehicle yaw; moreover, each vehicle has a rudder that facilitates high-speed tight turns. Basing on the model for ASVs in [25], and considering the under-actuated propulsion system of our vehicles, the LLC for the ASVs used herein is designed following the approach proposed in [32] and then used successfully in [12]. However, with respect to the approach proposed in [12], a partial force compensation related to the hydrodynamic effect of the rope connected to the vehicles has been added.

The LLC in [12] is expressed as the sum of a heading autopilot and a surge control aimed at causing the vehicle to follow the velocity reference commands given by the NSB. Indeed, following the control architecture of Fig. 3 and based on the sketch in Fig. 5, the output of the NSB for a single robot is a velocity vector  $\mathbf{U}_{NSB}$  that can be geometrically represented through its norm  $\|\mathbf{U}_{NSB}\|$  and its direction  $\chi_{NSB}$ . These are given to the low-level control as desired surge and heading/advancing direction. The heading autopilot is designed to control the heading of the vehicle to make it move in the desired direction  $\chi_{NSB}$ ; it regulates the propulsion torque and the rudder angle to correct the orientation of the vehicle. The surge control has to make the norm velocity of the vehicle to track the  $\|\mathbf{U}_{NSB}\|$  value generated by the NSB; however, the vehicle moves at full speed only when the orientation error is zero. Thus, the surge control works as a PI control regulating the advancing direction multiplied by a scaling factor depending on the orientation error.

Due to the presence of the floating rope connected to the vehicles, the LLC presented in [12] needs to be modified for the mission here. In fact, as we tested in preliminary field experiments, the rope applies a force on each vehicle that significantly affect its dynamics, reducing the maximum velocity and introducing noise in its motions. This is particularly significant as the vehicle velocity increases and thus cannot be neglected. To properly compensate the rope effects, we have to model the rope shape and the amplitude of the applied force on each vehicle.

We next present a model based on hydrodynamic consideration of the rope shape and of the applied force evaluation following which the associated control compensation is described. It is worth noticing that we consider the force applied by the rope due to the relative motion between the ASVs and the water. For simplicity, we will consider still water and absolute velocity of the ASVs; in the presence of current, instead, similar computation can be done using the relative velocity among ASVs and water.

When the rope is in tension, the rope shape can be expressed as a catenary. Such a shape is usually used to model a pendant rope subject to loading under gravity. As reported in [33], a rope in uniform cross flow reaches the same shape independently of the velocity of the fluid or the nature of the fluid itself (similarly to the case of the pendant rope, the shape is independent of the rope weight). Thus, in the simplified case in which the vehicles are in a rigid formation at a constant velocity (so as to suppose a uniform cross flow of water across the rope), the rope shape is expressed by a catenary:

$$y = \frac{1}{k} \cosh(x + \alpha) + \beta. \quad (9)$$

This curve represents the generic equation of a catenary in the case where the fluid is moving in the negative  $Y$  direction and the axis origin is in the centroid of the two vehicles. Thus, in our case, the fluid comes from the direction opposite to the team centroid velocity.

In Eq. 9, the parameters  $k$ ,  $\alpha$  and  $\beta$  depend on the relative positions of the vehicles with respect to the water, and on the length of the rope. It is possible to find the parameters  $k$ ,  $\alpha$  and  $\beta$  that define the shape of a rope of a given length  $L$  and whose extremes have coordinates  $[a \ b]^T$  and  $[-a \ -b]^T$ . The parameters are given by solving the system of three equations:

$$\sinh(ka) = \frac{1}{2}k\sqrt{L^2 + 4b^2} \quad (10)$$

$$\alpha = \frac{1}{k} \tanh^{-1} \left( \frac{2b}{L} \right) \quad (11)$$

$$\beta = b - \frac{1}{k} \left[ ka + \tanh^{-1} \left( \frac{2b}{L} \right) \right]. \quad (12)$$



The geometric shape of the rope in the uniform cross flow does not depend on other parameters e.g., the water velocity and viscosity, or the rope section dimension. These parameters, instead, affect the amplitude of the forces  $F_A$  and  $F_B$  respectively applied at the extremes A, B. These forces, equal to the tension in the rope at those points, are calculated by a balance of forces acting on the system. Neglecting frictional effects, the external force is due to the drag force acting on the rope. This can be calculated knowing the velocity of the fluid  $v_{inf}$ , the fluid’s Reynolds number  $Re$  and density  $\rho$ , and the geometric parameters of the rope (diameter of the rope  $d$ , its shape and its length). In particular, given the point A and B as in Fig. 7, the flow generates a force in the  $-Y$  direction equal to:

$$F_{\infty} = \frac{\rho}{2} C_D v_{inf}^2 \mathcal{A} \tag{13}$$

where  $C_D$  is the drag coefficient, the area of attack  $\mathcal{A}$  is given by  $2ad$ .

In our experiments we have used a rope of length of 20 m with a diameter of approximately 1 cm. Thus, given a Reynolds number of 34,000 (calculated considering that the maximum velocity of the vehicles is  $\sim 1.5$  m/s), the drag coefficient  $C_D = 1$  (Table 2.4 in [31]).

Given the points A, B and Eq. 9, we can calculate the area of attack  $\mathcal{A}$  of the fluid on the rope ( $\|2a\|$  is the norm of the projection along X of the  $|AB|$  vector). Moreover, from  $\dot{y}(-a)$  and  $\dot{y}(a)$ , we can calculate the angles of the curve at A and B. Since the forces applied to the vehicles at A and B are in the tangential direction to the rope, these give the directions respectively of the force vectors  $F_A$  and  $F_B$ . The amplitudes of  $F_A$  and  $F_B$  can finally be calculated by the balance of force among  $F_{\infty}$ ,  $F_A$  and  $F_B$ :

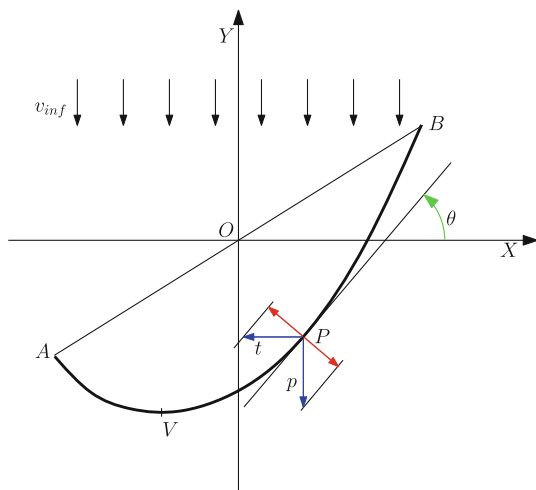


**Fig. 7** Catenary shape when fluid is moving in the  $-Y$  direction and the rope is fixed at A and B

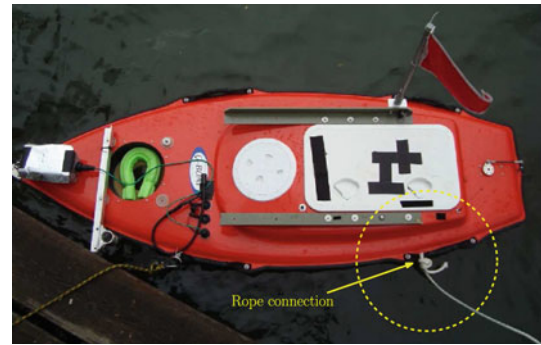


**Fig. 8** Connection of the rope to the vehicle

$$F_{A,x} + F_{B,x} = 0 \tag{14}$$

$$F_{A,y} + F_{B,y} = F_{\infty} \tag{15}$$

Finally, given the geometric details of the vehicles and the point where the rope is connected with respect to the vehicle centroid, it is possible to estimate the force and torque applied by rope in each vehicles’ centroid reference frame (see Fig. 8). Depending on the actuation system of the available vehicles, it is possible to compensate either the complete force or its partial components thereby reducing the effect of the rope on the LLC performance.

In our case, since the vehicles are underactuated we can only compensate for the force in the vehicles’ surge direction and the torque with respect to the centroid. Since the testbed vehicles have fins on the bottom of the hull these reduce the effect of rope force in the lateral direction (and the corresponding torque), in our experiment we decided to compensate only the force component in the surge direction. In particular, the compensation is applied as a feedforward term to the force in the advancing direction that is computed, onboard each vehicle, based on the position of the other vehicle and on the desired centroid velocity given from the NSB.

To validate the force estimation model, we have performed some tests by remotely controlling the ASVs connected with the floating rope. Repeatedly moving the vehicles in fixed formation with different inter-vehicle distances (so as to change the attack area), measuring the vehicles’ velocity and roughly knowing the force amplitude generated by the thrusters, from the test results we consider the approximation model coherent with our system performance.

### 6 Simulations

In this section, we present two simulation case studies of the overall mission execution. The first simulation shows ‘normal’ execution when the target is properly captured in the first attempt. The second simulation shows a case were the target is not captured at the first opportunity. In this case, we

force the transition of the supervisor state in order to test the recovery strategy. The recovery strategy can be useful in real mission execution when the target is not caged e.g., due to the presence of currents and sensor noise. It can be extended to the case when the target is lost during transportation.

The simulations are mainly aimed at testing the vehicles' coordination strategy, and they have been performed using part of the control code that is used for the field experiments. In particular, since the focus of the simulations is on the coordination strategy, some effects e.g., dynamic effects, sensor noise, wind and current effects, and hydrodynamic effects due to the presence of the rope have been neglected. Referring to Fig. 3, the simulation code uses the Supervisor and NSB blocks used for the real experiments, while it uses a unified and simplified block for the vehicles' dynamics/low level control that takes into consideration the under-actuated nature of the available vehicles. Vehicle dynamics and hydrodynamic effects of the floating rope are all taken into account in the real mission execution, as described in the next section.

The following parameters for the NSB behavior functions have been used in the simulations:

Centroid	$A_b = 0.1 \times I_2$
Orientation	$\lambda_o = 1.0$
Distance	$\lambda_d = 1.0$
Cross	$\lambda_c = .2$

Since the floating rope has a length of 20 m, the distance behavior function is activated when the inter-vehicle distance is greater than 16 m, and collision avoidance is activated when the inter-vehicle distance is less than 8 m.

### 6.1 One shot execution

In the first simulation case study, we present a standard execution of the mission where the target is considered captured at the first trial. The vehicles are commanded to cage a target positioned at  $[5 \ -32]^T$  m, and to bring it to goal at  $[12 \ -23]^T$  m.

Figure 9a shows the paths of the vehicles during the execution. After the software initialization and synchronization (supervisors' states "1-Wait Synchro"), the vehicles start their motion with an initialization maneuver (supervisors' states "2-Init. Maneuver") causing the floating rope getting in tension. This behavior commands the vehicles to keep the current formation orientation and to move their centroid in the formation advancing direction. Figure 9b, c shows the centroid and the orientation behavior function errors. From the first seconds of the execution traces, it is worth noticing that, during the initialization maneuver, the orientation behavior function error is deactivated (as indicated by the bold black line in the Fig. 9c), while a constant velocity is commanded by imposing a constant desired centroid offset

that moves the vehicles in the formation advancing direction.

When the current centroid is more than 5 m from the initial configuration, the supervisors' states switch to "3-Approach Target" and the target position is given as the desired centroid value; in this supervisor state, the desired formation angle computed as the centroid-target direction. This ensures that the vehicles approach the target from a direction appropriate for capture. From Fig. 9d, it is possible to observe the behavior function error behavior that approaches zero from  $\approx 18 - 80$  s. It is worth noticing that according to the behaviors priority orders, the orientation error converges to zero faster than the centroid error.

When the distance between the centroid of the formation and the target is lower than 5 m, the supervisors' states switch to "4-Cage target" and the vehicles are commanded to overtake the target (assigning a new centroid position in the advancing direction of the formation) keeping the current orientation. In the proper execution case (this simulation), the target is considered as caged. In the case the target passes outside the vehicle formation, a fault recovery strategy should be activated, this is discussed in the next subsection.

In the normal execution case, when the vehicles overtake the target by a few meters, the supervisors' states switch to "5-Toward goal" and the vehicles are commanded to transport the target to the goal. During their motions, the vehicles have to avoid maneuvers that would cause the target to be lost. Moreover, as shown in Fig. 9d, the distance between the vehicles is always such that it ensures collision avoidance and rope integrity.

### 6.2 Simulation with fault recovery strategy

The second simulation is analogous to the first one in the mission scope, the initial positioning of the vehicles, and in target and goal locations; however, when the vehicles are overtaking the target (supervisors' states "4-Cage target"), the supervisors are forced via software, so that they consider the target not properly caged. In this case, as shown in Fig. 10a, the vehicles are commanded to move far from the target (deactivating the orientation behavior function), rotate the formation to assume an approach angle appropriate for capture, and then try again to cage the target.

Figure 10b, c show the behavior function errors for this simulation case. It is worth noticing that, when the supervisors enter in the state "7-Rotate formation", the centroid behavior is deactivated (as indicated by the bold black line in the Fig. 10b), while a fixed desired orientation is given as a step reference (explaining the step error in Fig. 10c).

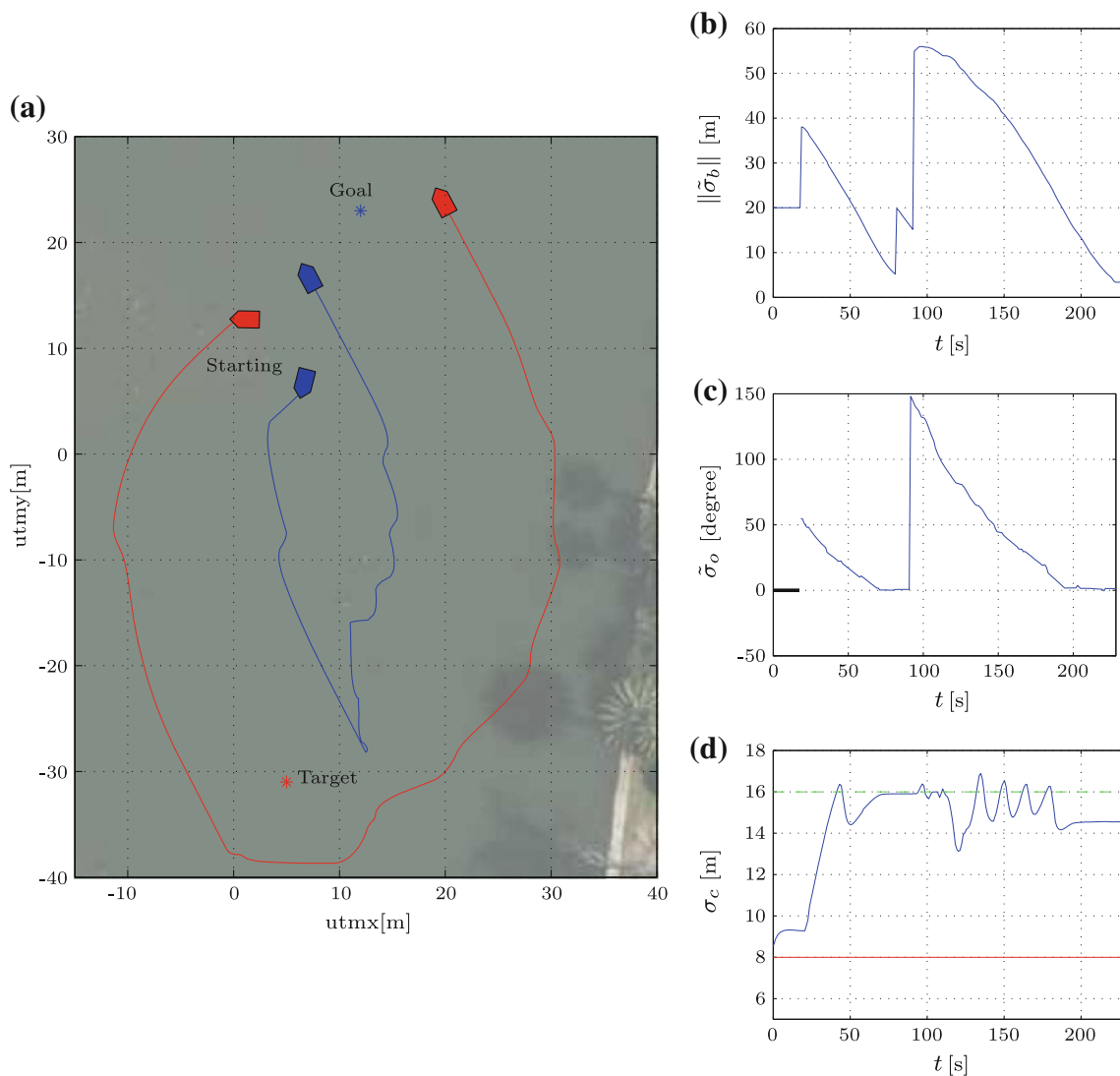


**Fig. 9** First simulation: **a** paths followed by the vehicles, **b** norm of the centroid behavior function, **c** error of the orientation behavior function, **d** distance between the vehicles

## 7 Experiments

### 7.1 Experimental set-up

The experimental testbed (Fig. 11) is composed of two ASVs designed by the University of Southern California’s Robotic Embedded Systems Lab (RESL). Each ASV is an Ocean-Science QBoat-I hull with a length of 2.1 m and a width of 0.7 m at the widest section. Each ASV weighs 48 kg with instrumentation and batteries. The onboard computing package consists of a Mini-ITX 2 GHz dual-core computer. A 28 Ah sealed lead acid (SLA) battery is used to power the computer and all sensors, and a 32 Ah AGM battery is used for the drive motors and the rudder. The vehicles have a nominal runtime of 6 h.

The vehicle sensor suite used in the experiments reported here is a navigation package. Both vehicles are equipped with

a u-blox EVK-5H GPS that provides global position updates at 2 Hz, and a Microstrain 3DM-G IMU with integrated compass sampled at 50 Hz.

The ASVs are controlled by software built using the open-source framework Robot Operating System (ROS) [36]. ROS provides a structured communications layer on top of the operating system, allowing intercommunicating nodes and services to be developed easily. We developed the different nodes of the ASVs to manage specific portions of the system or of the control architecture as reported in Fig. 12.

### 7.2 Experimental results

The experiments were performed in Echo Park Lake in Los Angeles (lat. 34°4’22.06’’N, long. 118°15’38.74’’W) to validate the proposed strategy in the field. Preliminary experiments presented in [13] validate the coordination strategy,

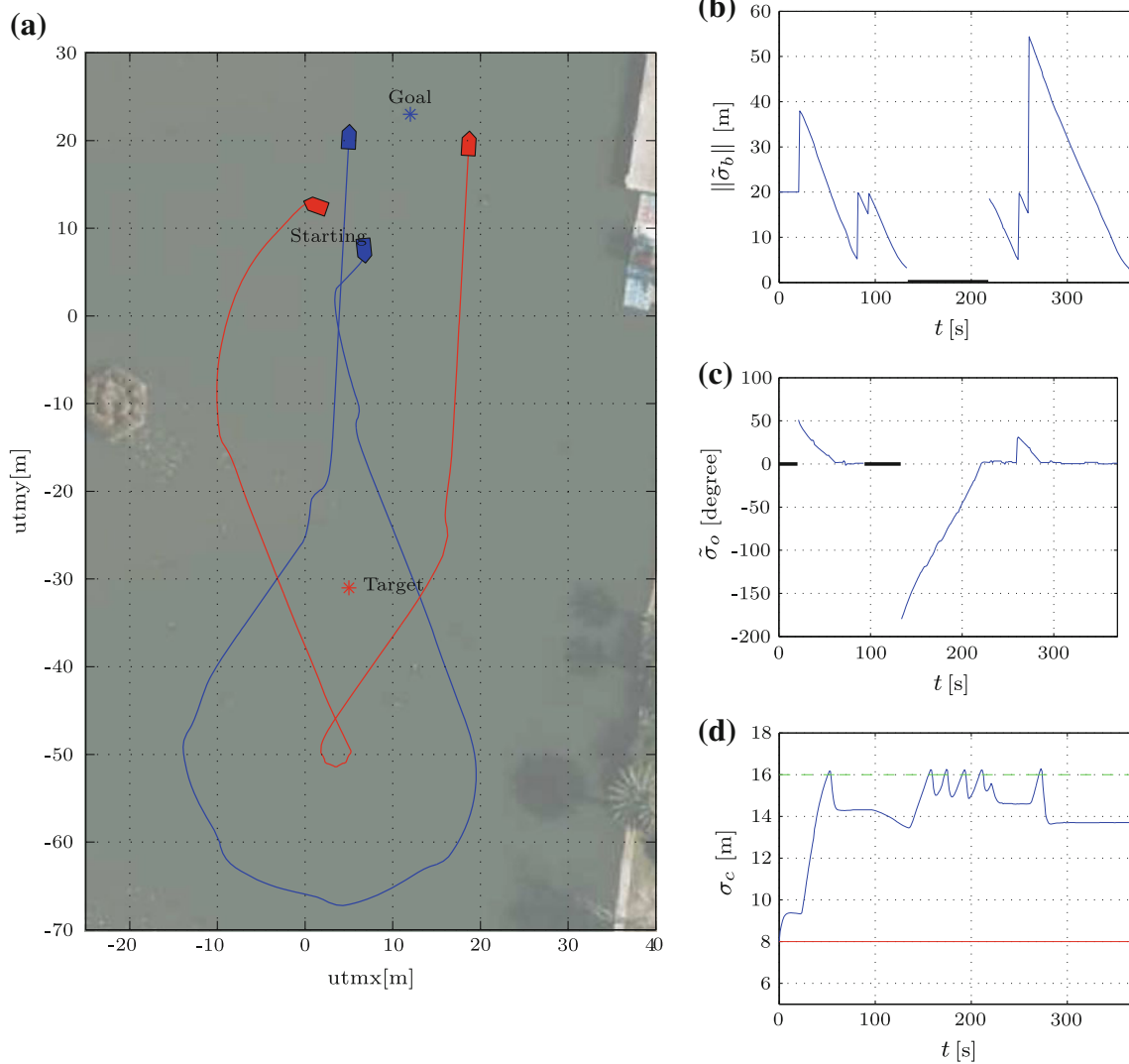


**Fig. 10** Second simulation: **a** Paths followed by the vehicles, **b** norm of the centroid behavior function, **c** error of the orientation behavior function, **d** distance between the vehicles



**Fig. 11** The USC RESL Autonomous Surface Vehicles connected with a floating rope

however in that case the ASVs were not connected with the rope and the caging was not really executed. In this section, instead, we report the first complete execution of the mission in the field and the first test of the the LLC with force com-

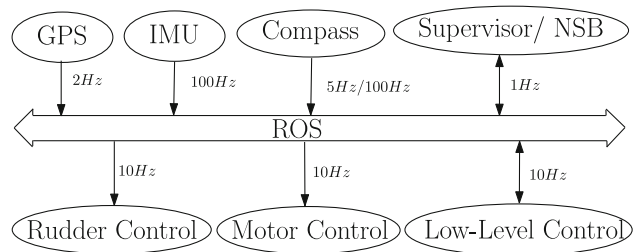


**Fig. 12** Software architecture onboard each vehicle

pensation. For the real mission, a floating target was built and equipped with a GPS and wireless communication devices; thus, its position was continually transmitted to the vehicles over a wireless link. The parameters of the behavior functions' gains were selected as shown in the following table:

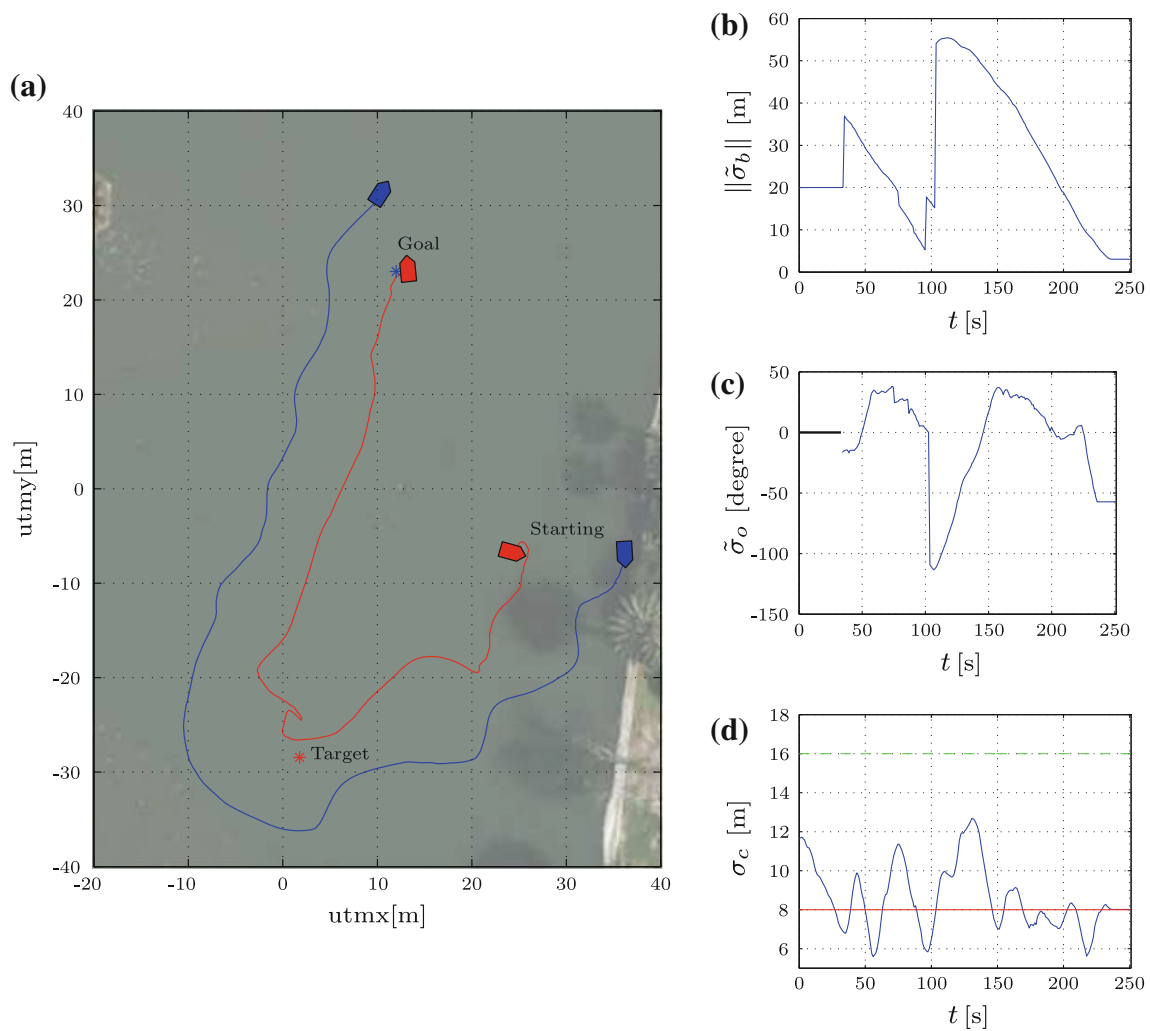


**Fig. 13** Experiment: **a** paths followed by the vehicles, where the *bottom* and *top stars*, respectively represent the initial position of the target and the goal. **b** Norm of the centroid behavior function. **c** Error of the orientation behavior function. **d** Distance between the vehicles

Centroid	$\Lambda_b = 0.1 \times I_2$
Orientation	$\lambda_o = 1.0$
Distance	$\lambda_d = 1.0$
Cross	$\lambda_c = .2$

Figure 13.a shows the paths of the vehicles during the overall mission. At the beginning of the mission, the supervisors synchronize to cause the vehicles to start moving at the same time. The vehicles start the initialization maneuver which causes the rope to get in tension. Next, the vehicles move toward the target (the bottom star in Fig. 13a) keeping a distance lower than 20 m at all times. The desired orientation angle of the formation is given by the centroid-target direction. Once the centroid behavior function error is lower than 3 m, the supervisors switch to the respective next states, and command the vehicles to continue to move along their current direction. As previously explained, this causes the vehicles to overtake the target and to ensure that it has been

properly captured. At this stage the target is caged. Next, the supervisors command the vehicles to move toward the goal (the top star in Fig. 13a). To avoid losing the target during the transport phase the vehicles are not allowed to move backwards with respect to the angle of the formation. The vehicles stop when the distance from the goal is less than 3 m.

Figure 13b, c shows the error of the centroid behavior function during the complete experiment. From the Figure, the different states of the supervisors can be recognized. In the first 30 s, the vehicles perform a low velocity initialization maneuver, then the vehicles move toward the target reducing the behavior function error. When the supervisor state changes, a new position in the vehicles’ advancing direction is commanded to ensure that the target is properly caged (this causes a step in the centroid error); the vehicles move in this new direction until the distance from the centroid and the initial position of target is greater than 5 m (around 105 s). Next, the supervisors switch again and assign the designated

position as the desired value of the centroid behavior function (causing a new step to the centroid error). The overall mission ends when the vehicles' centroid reaches the goal.

Figure 13c shows the orientation error during the overall mission. Figure 13d shows the distance between the vehicles during the experiment; the distance behavior function is activated when the distance is greater than 16 m while collision avoidance is activated when the distance is less than 8 m. It is worth noticing that we use standard GPS for position estimation. With a more specific relative position estimation system (with higher accuracy and frequency), e.g. based on local sensors as sonar or camera, better performance can be achieved in term of accuracy and promptness of response; however, the successful mission execution with low performance sensors proves the robustness of the approach to work in the field.

The video attached to the paper shows the experiment in progress at Echo Park lake.

## 8 Conclusions

In this paper, we introduce the problem of caging and transport of floating objects on the water surface using cooperating aquatic ASVs.

We developed a coordination control strategy for two autonomous vehicles to achieve the assigned mission in a cooperative way. Given the complexity of the problem, we organized the control architecture in a hierarchical multi-layered structure to keep the low level control problems separate from the supervisory ones. The core of the control strategy is composed of the NSB control that allows the system to simultaneously deal with multiple behaviors arranged in priority; this approach, taking the advantages of behavior based techniques, allows the system to deal with dynamic and unpredicted scenarios.

The overall control strategy has been tested in simulations and with experiments in the field. Two under-actuated ASVs were connected with a floating rope and were used to cage and transport a floating target on the surface of a lake. To properly conduct experiments on the water surface, several aspects have been considered while developing the control strategy.

For example, we find that the hydrodynamic effects of the rope strongly affects the performance of the vehicles and cannot be neglected. The presence of the rope in fact significantly reduces the maximum velocity of the vehicles and introduces noise in their motions; moreover, we realized that its effects are extremely difficult to model and predict. In the paper we presented a simplified scheme to estimate this force based on the dimension of the rope, the relative positioning of the vehicles and their velocity. The successful execution of the mission supports its effectiveness.

In future works, we will add the obstacle avoidance functionality; in the performed experiments, in fact, we have only considered the collision avoidance between the vehicles, while external obstacles have been neglected. It is worth noting that, since the vehicles are connected with the rope, they will be commanded to cooperatively move around the obstacle, thus avoiding the situation where the obstacle gets stuck in the rope. In ongoing work, we are extending this approach to the case where the vehicles move at unequal speeds and cage a deformable object, as might be the case in an oil skimming operation on the water surface.

**Acknowledgments** This work was supported in part by the NOAA MERHAB program under grant NA05NOS4781228 and by NSF as part of the Center for Embedded Network Sensing (CENS) under grant CCR-0120778, by NSF grants CNS-0520305 and CNS-0540420, by the ONR MURI program (grants N00014-09-1-1031 and N00014-08-1-0693) by the ONR SoA program and a gift from the Okawa Foundation. The research leading to these results has received funding from the European Community's Seventh Framework Programme under grant agreement n. 231378 (STREP project Co<sup>3</sup>AUVs - Cognitive Cooperative Control for Autonomous Underwater Vehicles) and from the Italian Government, under Grant FIRB - Futuro in ricerca 2008 n. RBFR08QWUV (project NECTAR).

## References

1. Aguiar A, Almeida J, Bayat M, Cardeira B, Cunha R, Hausler A, Maurya P, Oliveira A, Pascoal A, Pereira A, Rufino M, Sebastiao L, Silvestre C, Vanni F (2009) Cooperative autonomous marine vehicle motion control in the scope of the EU GREX project: theory and practice. In: Proceedings IEEE Conference Oceans'09, Bremen, D
2. Aguiar A, Hespanha JP (2007) Trajectory-tracking and path-following of underactuated autonomous vehicles with parametric modeling uncertainty. *IEEE Trans Autom Control* 52(8):1362–1379
3. Aguiar A, Pascoal AM (2007) Dynamic positioning and way-point tracking of underactuated AUVs in the presence of ocean currents. *Int J Control* 80(7):1092–1108
4. Antonelli G (2009) Stability analysis for prioritized closed-loop inverse kinematic algorithms for redundant robotic systems. *IEEE Trans Robotics* 25(5):985–994
5. Antonelli G, Arrichiello F, Chiaverini S (2008) The entrapment/escorting mission: an experimental study using a multi-robot system. Special Issues on Design, Control, and Applications of Real-World Multi-Robot Systems. *IEEE Robotics Autom Mag (RAM)* 15(1):22–29
6. Antonelli G, Arrichiello F, Chiaverini S (2008) The Null-Space-based Behavioral control for autonomous robotic systems. *J Intell Service Robotics* 1(1):27–39
7. Antonelli G, Arrichiello F, Chiaverini S (2008) Stability analysis for the Null-Space-based Behavioral control for multi-robot systems. In: 47th IEEE Conference on Decision and Control and 8th European Control Conference, Cancun, MEX
8. Antonelli G, Arrichiello F, Chiaverini S (2009) Experiments of formation control with multirobot systems using the Null-Space-based Behavioral control. *IEEE Trans Control Syst Technol* 17(5):1173–1182
9. Arkin RC (1989) Motor schema based mobile robot navigation. *Int J Robotics Res* 8(4):92–112

10. Arkin RC (1998) Behavior-based robotics. The MIT Press, Cambridge
11. Arrichiello F, Chiaverini S, Indiveri G, Pedone P (2010) The null-space based behavioral control for mobile robots with velocity actuator saturations. *Int J Robotics Res* 29(10):1317–1337
12. Arrichiello F, Das J, Heidarsson H, Pereira A, Chiaverini S, Sukhatme GS (2009) Multi-robot collaboration with range-limited communication: experiments with two underactuated ASVs. In: Proceedings 2009 international conference on field and service robots, Cambridge, July
13. Arrichiello F, Heidarsson H, Chiaverini S, Sukhatme GS (2010) Cooperative caging using autonomous aquatic surface vehicles. In: Proceedings 2010 IEEE International Conference on Robotics and Automation, pp 4763–4769, Anchorage, May
14. Ashrafiuon H, Muske KR, McNinch LC, Soltan RA (2008) Sliding-mode tracking control of surface vessels. *IEEE Trans Ind Electron* 55(11):4004–4012
15. Bandyopadhyayand T, Sarcione L, Hover F (2009) A simple reactive obstacle avoidance algorithm and its application in Singapore harbour. In: Proceedings 2009 International Conference on Field and Service Robots, Cambridge, July
16. Borhaug E, Pavlov A, Ghabcheloo R, Pettersen K, Pascoal A, Silvestre C (2006) Formation control of underactuated marine vehicles with communication constraints. In: Proceedings 7th IFAC Conference on Manoeuvring and Control of Marine Craft, Lisbon
17. Brooks RA (1986) A robust layered control system for a mobile robot. *IEEE J Robotics Autom* 2(1):14–23
18. Cheng P, Fink J, Kim S, Kumar V (2009) Cooperative towing with multiple robots. *Algorithmic Foundation of Robotics VIII*, pp 101–116
19. Curcio J, Leonard J, Patrikalakis A (2005) SCOUT-a low cost autonomous surface platform for research in cooperative autonomy. In: Proceedings of MTS/IEEE, OCEANS, 2005, pp 725–729, Washington
20. Dong W, Farrell JA (2008) Formation control of multiple underactuated surface vessels. *Control Theory Appl IET* 2(12):1077–1085
21. Esposito J, Feenster M, Smith E (2008) Cooperative manipulation on the water using a swarm of autonomous tugboats. In Proceedings 2008 IEEE International Conference on Robotics and Automation, pp 1501–1506. IEEE
22. Esposito JM (2010) Decentralized cooperative manipulation with a swarm of mobile robots: the approach problem. In: American Control Conference (ACC), 2010, pp 4762–4767
23. Fahimi F (2007) Sliding-mode formation control for underactuated surface vessels. *IEEE Trans Robotics* 23(3):617–622
24. Fink J, Hsieh MA, Kumar V (2008) Multi-robot manipulation via caging in environments with obstacles. In: Proceedings IEEE International Conference on Robotics and Automation, pp 1471–1476, Pasadena
25. Fossen TI (2002) Marine control systems: guidance, navigation and control of ships, rigs and underwater vehicles. Marine Cybernetics, Trondheim
26. Gerkey BP, Mataric MJ (2002) Sold!: Auction methods for multi-robot coordination. *IEEE Trans Robotics Autom* 18(5):758–768
27. Ghommam J, Mnif F (2009) Coordinated path following control for a group of underactuated surface vessels. *IEEE Trans Ind Electron* 56(10):3951–3963
28. Ihle IAF, Jouffroy J, Fossen TI (2006) Robust formation control of marine craft using lagrange multipliers. In: Pettersen KY, Gravdahl T, Nijmeijer H (eds) Group coordination and cooperative control. Springer-Verlag's Lecture Notes in Control and Information Systems series, May
29. Kube CR, Bonabeau E (2000) Cooperative transport by ants and robots. *Robotics Auton Syst* 30(1–2):85–101
30. Lefeber EL, Pettersen KY, Nijmeijer H (2003) Tracking control of an underactuated ship. *IEEE Trans Control Syst Technol* 11(1):52–61
31. Newman JN (1977) Marine hydrodynamics. MIT Press, Cambridge
32. Pereira A, Das J, Sukhatme GS (2008) An experimental study of station keeping on an underactuated ASV. In: 2008 IEEE/RSJ International Conference on Intelligent Robots and Systems, Nice, France, September
33. Peters F (2000) Shape and drag of a bulging rope in uniform cross flow. *Acta Mechanica* 139(1):161–170
34. Pettersen KY, Fossen TI (2000) Underactuated dynamic positioning of a ship-experimental results. *IEEE Trans Control Syst Technol* 8(5):856–863
35. Pettersen KY, Mazencs F, Nijmeijer H (2004) Global uniform asymptotic stabilization of an underactuated surface vessels: experimental results. *IEEE Trans Control Syst Technol* 12(6):891–903
36. Quigley M, Gerkey B, Conley K, Faust J, Foote T, Leibs J, Berger E, Wheeler R, Ros ANg (2009) An open-source robot operating system. In: Open-source software workshop of the 2009 IEEE International Conference on Robotics and Automation, Kobe
37. Shafer AJ, Benjamin MR, Leonard JJ, Curcio J (2008) Autonomous cooperation of heterogeneous platforms for sea-based search tasks. In: Proceedings MTS/IEEE OCEANS 2008, Quebec
38. Wang Z, Nakano E, Takahashi T (2003) Solving function distribution and behavior design problem for cooperative object handling by multiple mobile robots. *IEEE Trans Syst Man Cybernet Part A* 33(5):537–549